Article

Diversity of Magneto-Aerotactic Behaviors and Oxygen Sensing Mechanisms in Cultured Magnetotactic Bacteria

Christopher T. Lefèvre,[1,3] Mathieu Bennet,[1] Livnat Landau,[1,2] Peter Vach,[1] David Pignol,[3] Dennis A. Bazylinski,[4] Richard B. Frankel,[5] Stefan Klumpp,[2] and Damien Faivre[1,*]

[1]Department of Biomaterials and [2]Department of Theory and Bio-Systems, Max Planck Institute of Colloids and Interfaces, Potsdam, Germany; [3]CEA/CNRS/Aix-Marseille Université, UMR7265 Biologie Végétale et Microbiologie Environnementales, Laboratoire de Bioénergétique Cellulaire, Saint Paul lez Durance, France; [4]University of Nevada at Las Vegas, School of Life Sciences, Las Vegas, Nevada; and [5]Department of Physics, California Polytechnic State University, San Luis Obispo, California

ABSTRACT Microorganisms living in gradient environments affect large-scale processes, including the cycling of elements such as carbon, nitrogen or sulfur, the rates and fate of primary production, and the generation of climatically active gases. Aerotaxis is a common adaptation in organisms living in the oxygen gradients of stratified environments. Magnetotactic bacteria are such gradient-inhabiting organisms that have a specific type of aerotaxis that allows them to compete at the oxic-anoxic interface. They biomineralize magnetosomes, intracellular membrane-coated magnetic nanoparticles, that comprise a permanent magnetic dipole that causes the cells to align along magnetic field lines. The magnetic alignment enables them to efficiently migrate toward an optimal oxygen concentration in microaerobic niches. This phenomenon is known as magneto-aerotaxis. Magneto-aerotaxis has only been characterized in a limited number of available cultured strains. In this work, we characterize the magneto-aerotactic behavior of 12 magnetotactic bacteria with various morphologies, phylogenies, physiologies, and flagellar apparatus. We report six different magneto-aerotactic behaviors that can be described as a combination of three distinct mechanisms, including the reported (di-)polar, axial, and a previously undescribed mechanism we named unipolar. We implement a model suggesting that the three magneto-aerotactic mechanisms are related to distinct oxygen sensing mechanisms that regulate the direction of cells' motility in an oxygen gradient.

INTRODUCTION

Microaerophilic microorganisms thrive at the oxic-anoxic interface (OAI) in aquatic environments. This niche represents a tiny layer of ~100 μm in thickness but is a very coveted zone due to the overlap of reduced and oxidized chemical species. For instance, microorganisms that use reduced sulfur compounds as an energy source can find in this biotope an electron donor (e.g., sulfide) as well as a terminal electron acceptor (oxygen). This layer is thus a hot spot for microorganismal adaptation (1). Evidence of specific adaptations for exploiting oxygen gradients includes the high swimming speeds of many bacteria, whose mean velocities often exceed 60 to 80 μm s^{-1} (2).

Another adaptation by bacteria that inhabit this layer is the biomineralization of magnetic nanoparticles and their organization in chains to comprise a permanent magnetic dipole in each cell. This biological adaptation has been associated with an enhanced capacity to rapidly find the microaerobic zone, a behavior termed magnetotaxis (3). Microorganisms displaying magnetotaxis are the magnetotactic bacteria (MTB). The organelles responsible for the magnetotactic behavior are referred to as magnetosomes. They consist of magnetite (Fe_3O_4) or greigite (Fe_3S_4) particles surrounded by a biomembrane (4–6) and whose formation and arrangement is under genetic and biochemical control. Magnetite producers are generally localized at the OAI (7). MTB orient and navigate along the Earth's geomagnetic field lines (3). North-seeking (NS) MTB predominate in the Northern Hemisphere, whereas in the Southern Hemisphere, they are predominantly south-seeking (SS) (8). However, magnetotaxis is not considered as a true taxis, but rather a magnetically assisted aerotaxis, also referred to as magneto-aerotaxis, directing the cells to a preferred oxygen concentration (9). The magnetic field passively orients the cells, which in turn actively swim using their flagellar apparatus. Aerotaxis determines where the downward and upward migrations stop in oxygen gradient biotopes. Thus, in both hemispheres magnetotaxis reduces the three-dimensional random walk associated with aerotaxis to a one-dimensional search, supposedly yielding an energy advantage over nonmagnetotactic organisms (10). MTB migrate toward the oxic-anoxic interface; once this preferred microhabitat is reached, migration stops but cells continue swimming along the field within the aerotactic band (9) at the oxic-anoxic interface, and alternate swimming parallel to the field with swimming antiparallel to the field. In general, magnetotaxis enables a bacterium to swim in a straight line without losing its heading due to rotational diffusion.

Submitted March 28, 2014, and accepted for publication May 29, 2014.

*Correspondence: damien.faivre@mpikg.mpg.de

Editor: Stefan Diez.

0006-3495/14/07/0527/12 $2.00

http://dx.doi.org/10.1016/j.bpj.2014.05.043

Two different magneto-aerotactic mechanisms have been proposed for *Magnetococcus marinus* strain MC-1 and *Magnetospirillum magnetotacticum* strain MS-1 (9). Strain MC-1, which swims persistently in one direction along the magnetic field **B** under oxic conditions, is polar magneto-aerotactic (NS or SS). Strain MS-1 as well as other *Magnetospirillum* species grown in liquid medium with a homogeneous oxygen concentration swim in either direction along **B** with frequent, spontaneous reversals of swimming direction. They are classified as axial magneto-aerotactic. The distinction between NS and SS does not apply to axial magneto-aerotactic bacteria. Polar MTB use **B** as an axis and a direction of motility, whereas axial MTB use **B** only as an axis of motility (9). The difference between polar and axial magnetotaxis is more obvious when cells are transferred into a microcapillary containing an oxygen gradient. Both polar and axial cells form a microaerobic band if the local magnetic field is antiparallel to the oxygen gradient (position in Northern Hemisphere environments). The distinction between polar and axial is evidenced when **B** is reversed and positioned parallel to the oxygen gradient. In such conditions, the axial MTB perform a U-turn when the field is reversed, and continue to form a microaerotactic band. In contrast, the microaerotactic band formed by cells of strain MC-1 rapidly disperses when the magnetic field is rotated 180° (9).

We studied the aerotactic responses of 12 different species of MTB, part of which were only recently cultivated (4). The strains exhibit varying properties (Table 1). We found that all these species of MTB form a microaerotactic band at the OAI at a preferred oxygen concentration ranging from 0 to 25 μM (as a comparison, the oxygen concentration at the air/water interface is 220 μM). Furthermore, the results indicate six different magneto-aerotactic behaviors indicating different aerotactic sensing mechanisms in MTB. Our results also illustrate the potential of MTB to decipher the mechanisms involved in other taxis.

MATERIALS AND METHODS

Growth of magnetotactic bacteria

Cells were grown in oxygen-gradient media as previously described (11), *Magnetospirillum gryphiswaldense* was also grown in liquid medium (12). A solution of 4% neutralized cysteine • HCl • $2H_2O$ was used as the reducing agent to allow the formation of the gradient. Strains MSR-1, UT-4, PR-1, MV-1, PR-2, LM-1, RS-1, and PR-3 were grown heterotrophically with succinate as the energy source, whereas strains MMS-1, SS-5, MC-1, and SS-1 were grown autotrophically with thiosulfate (MMS-1, SS-5, and MC-1) or sulphide (SS-1) as the energy source (see the Supporting Material). Sampling, isolation, and phylogenetic determination of the strains PR-1, PR-2, PR-3, and SS-1 are described in detail in the Supporting Material.

Capillary preparation

A drop of 200 μl of a bacterial culture sampled from the aerotactic band was added to 500 μl of a liquid medium of the same composition of the medium used for the culture and supplemented with 2.5 nM of the oxygen sensitive fluorophore (Tris(2,2′-bipyridyl)dichlororuthenium(II) hexahydrate, CAS No. 50525-27-4, Sigma-Aldrich). The magnetic separation occurred during 10–30 min (depending on the swimming speed of the strain) with two stirring magnets generating a magnetic field of 0.5 mT at the edges of the drop and placed around the drop to separate the north-seeking cells in the liquid medium. 100 μl of the north-seeking cells aggregated at the edge of the drop were then harvested, flushed 10 min with argon gas, and transferred by capillarity effect in a microcapillary (#3520-050, Vitrotubes). One side of the capillary was left open to allow oxygen diffusion in the sample and the other end of the capillary was sealed with petroleum jelly to avoid oxygen diffusion. This preparation resulted in the formation of an oxygen gradient in the microcapillary.

Light and electron microscopy

A custom-made light microscope specifically dedicated to provide a nonmagnetic platform that can accommodate the magnetic setup without possible disturbance due to magnetic pieces and the potential to implement multiple light sources and cameras was used (12) (see the Supporting Material). The microcapillary under the light microscope was exposed to a magnetic field of 50 μT (strength of the earth magnetic field) parallel to the long axis of the microcapillary.

Magnetosomes organization and flagellar apparatus were determined using a transmission electron microscope ZEISS EM 912 (Leica, Germany) at 100 kV. For flagella observation, the samples were stained for 1 min with 1% uranyl acetate.

Speed measurement

Responses of the bacteria in the microcapillary at the cell and population level were analyzed from high-speed videos recorded with the high-speed camera. The high speed videos were analyzed using custom-written code (MATLAB, R2011a, The MathWorks, Natick, MA). Bacteria were detected in video frames based on an intensity threshold, after background subtraction and Gaussian smoothing. Areas above or below a certain intensity threshold that were sufficiently large were identified as bacteria. After localizing the bacteria in each frame, the positions were grouped into trajectories. Tracks were split on reversal events. To measure the swimming speed we compared the position of the bacteria n frames apart. The measured average bacteria speed depended on the choice of the parameter n, because inaccuracies in the position estimate increase the measured speed when n is small. When n is large the measured speed is lower than the actual speed of the bacteria, following a curved trajectory. Because it was not obvious which value should be chosen for n, we determined speed values for all reasonable values of n and calculated a standard deviation that was incorporated into the estimate for the accuracy of the speed measurement. Speeds below a certain threshold were discarded to avoid including bacteria that were hampered in their normal swimming behavior.

Oxygen gradient measurement

The oxygen concentration along the capillary was measured using an oxygen-sensitive fluorescent probe (Tris(2,2′-bipyridyl)dichlororuthenium(II) hexahydrate, CAS No. 50525-27-4, Sigma-Aldrich) and epifluorescence wide-field fluorescence imaging. The sample was excited at 470 nm (pE-100, CoolLED) and the fluorescence collected through a bandpass filter by a fluorescence camera (NeoSCMOS, Andor). Calibration of the fluorescence intensity as a function of oxygen concentration was performed in situ using a capillary filled with medium and a capillary filled with oxygen-free medium. The oxygen of the medium was measured using an oxygen microprobe (12). The measurements of the two fluorescence intensities, I_0 and I_{100}, corresponding to the fluorescence intensity of the medium without and with oxygen, respectively, were used with the Stern-Volmer equation (12) to calculate the oxygen concentration in the capillary.

TABLE 1 Characteristics of the 12 magnetotactic bacteria under study

Name of the MTB strain (magneto-aerotactic behavior)	Morphology (shape/flagellar apparatus)	Taxonomy (class/order)	Physiology in microaerobic conditions/ electron donor/ biotope of origin	Magnetite shape	Reference	Transmission electron microscope micrograph (A. unstained, B. stained)
Magnetosopirillum gryphiswaldense strain MSR-1 (axial or mix of axial and dipolar)	Spirillum/ 2 polar flagella	*Alphaproteobacteria/ Rhodospirillales*	Chemoheterotrophy/ Succinate/ Freshwater river	cuboctahedral	(14)	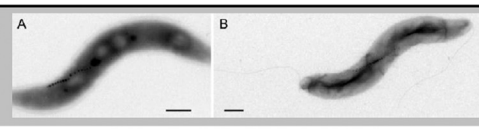
Strain UT-4 (dipolar)	Spirillum/ 2 polar flagella	*Alphaproteobacteria/ Rhodospirillales*	Chemoheterotrophy/ Succinate/ Freshawter pond	cuboctahedral	(19)	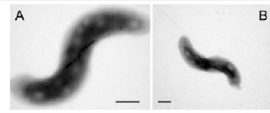
Magnetospira thiophila strain MMS-1 (dipolar)	Spirillum/ 2 polar flagella	*Alphaproteobacteria/ Rhodospirillales*	Chemoautotrophy/ Thiosulfate/ Salt marsh	elongated octahedral	(16)	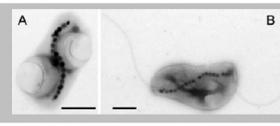
Strain PR-1 (mix of axial and unipolar directed towards the oxic zone)	Spirillum/ 2 polar flagella	*Alphaproteobacteria/ Rhodospirillales*	Chemoheterotrophy/ Succinate/ Marine	elongated octahedral	This study	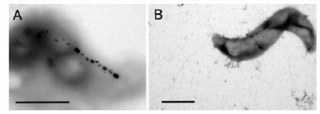
Magnetovibrio blakemorei strain MV-1 (unipolar directed towards the oxic zone)	Vibrio/ 1 polar flagellum	*Alphaproteobacteria/ Rhodospirillales*	Chemoheterotrophy/ Succinate/ Salt marsh	elongated octahedral	(15)	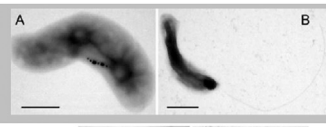
Strain PR-2 (dipolar)	Vibrio/ 1 polar flagellum	*Alphaproteobacteria/ Rhodospirillales*	Chemoheterotrophy/ Succinate/ Marine	elongated octahedral	This study	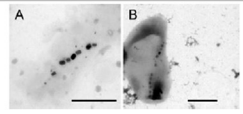
Strain LM-1 (dipolar)	Vibrio/ 1 polar flagellum	*Alphaproteobacteria/ Rhodospirillales*	Chemoheterotrophy/ Succinate/ Freshwater lake	elongated octahedral	(19)	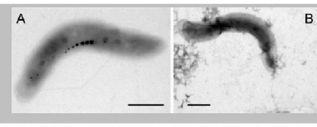
Strain SS-5 (unipolar directed towards the oxic zone)	Rod/ 1 polar flagellum	*Gammaproteobacteria/ Thiotricales*	Chemoautotrophy/ Thiosulfate/ Hypersaline lagoon	elongated octahedral	(20)	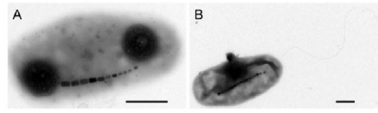
Desulfovibrio magneticus strain RS-1 (unipolar directed towards the anoxic zone)	Rod/ 1 polar flagellum	*Deltaproteobacteria/ Desulfovibrionales*	Chemoheterotrophy/ Succinate/ Freshwater river	anisotropic	(18)	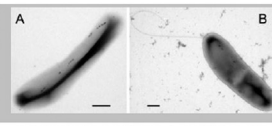
Magnetococcus marinus strain MC-1 (dipolar)	Cocci/ 2 bundles of 7 flagella	*Alphaproteobacteria/ Magnetococcales*	Chemoautotrophy/ Thiosulfate/ Estuary	elongated octahedral	(17)	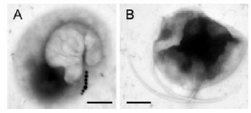
Strain PR-3 (dipolar)	Cocci/ 2 bundles of 7 flagella	*Alphaproteobacteria/ Magnetococcales*	Chemoheterotrophy/ Succinate/ Marine	elongated octahedral	This study	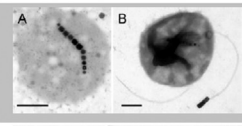
Strain SS-1 (dipolar)	Cocci/ 2 bundles of 7 flagella	*Alphaproteobacteria/ Magnetococcales*	Chemoautotrophy/ Sulfide/ Hypersaline lagoon	elongated octahedral	This study	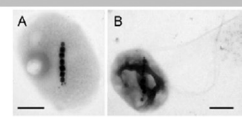

Cell distribution

Transmission images of the capillary were recorded every 100 μm, from the air/water interface to a few millimeters after the microaerotactic band, allowing the reconstruction of the bacteria density distribution along the capillary. The positions of bacteria in the obtained pictures were determined using custom-written code (MATLAB, R2011a, The MathWorks). Bacteria were detected based on an intensity threshold after background subtraction and Gaussian smoothing. Areas that were neither too big, nor too small were identified as bacteria and bacteria positions that were too close to

each other were combined into an average. At and close to the band, bacteria concentrations were so high, that individual bacteria positions could not be accurately determined and the number of measured positions saturated at a high value. Based on the obtained positions, we plotted histograms that indicate the distribution of the bacteria density.

Model for magneto-aerotaxis

Magneto-aerotaxis was modeled as a one-dimensional aerotaxis (12,13). The full model is given by three equations for the local number of bacteria moving to the left (ρ_R) and moving to the right (ρ_L) and for the local oxygen concentration (c):

$$\partial_t \rho_L = +v\partial_x \rho_L - k_{LR}\rho_L + k_{RL}\rho_R,$$

$$\partial_t \rho_R = -v\partial_x \rho_R - k_{RL}\rho_R + k_{LR}\rho_L,$$

$$\partial_t c = D\partial_x^2 c - k(c)(\rho_L + \rho_R).$$

These first two equations describe bacterial swimming (with velocity v) and reversals of the swimming direction (with rates k_{RL} and k_{LR}). The last equation describes the oxygen diffusion and oxygen consumption by the bacteria, where D is the diffusion of oxygen in water and $k(c) = \kappa\ c/c + c_0$ is the concentration-dependent consumption rate of the oxygen, as described in Bennet et al. (12). The sensing mechanism is taken into account by altering the rate of reversals of the swimming direction between a basal switching rate and an increased switching rate. These rates are determined separately for each regime (the oxic and the anoxic), by considering either the oxygen gradient, in case of axial mechanism, or the direction of the magnetic field, in case of dipolar mechanism. The increased value is applied for oxygen concentrations larger than the preferred oxygen concentration, if the swimming direction is either up the gradient, in case of axial sensing, or antiparallel to the magnetic field direction, in case of dipolar mechanism. For oxygen concentrations smaller than the preferred oxygen concentration (c^*), the increased switching rate is applied if the swimming direction is either down the gradient, in case of axial sensing, or parallel to the magnetic field direction, in case of dipolar mechanism. In case of unipolar mechanism, the bacteria's switching rate depends on the oxygen gradient in one regime and on the direction of the magnetic field in the other. The algorithm for determining the values of the switching rates is depicted in Fig. S1. As an example, we write out the dependence of the switching rates for the axial case:

$$k_{LR}(x) = k_{low} + \left(k_{high} - k_{low}\right)\theta(c(x), c'(x))$$

$$k_{RL}(x) = k_{low} + \left(k_{high} - k_{low}\right)[1 - \theta(c(x), c'(x))]$$

$$\text{with } c'(x) = \frac{dc(x)}{dx} \text{ and}$$

$$\theta(c(x), c'(x)) = \begin{cases} 1 & \text{if}(c(x)>c^* \text{ and } c'(x)<0) \\ & \text{or } (c(x)<c^* \text{ and } c'(x)>0) \\ 0 & \text{else.} \end{cases}$$

Parameter values used in the numerical calculations are shown in Table S1.

To mimic the conditions in the experiments, we numerically solved the equations by setting the initial distribution of the bacteria to be homogeneous, with equal probability of swimming to the left or to the right. The initial oxygen concentration corresponds to a situation of zero oxygen in the capillary at time zero and to an open end of the capillary through which the oxygen diffuses. The magnetic field direction is initially antiparallel to the direction of the oxygen gradient. Once the bacteria accumulate in the preferred oxygen concentration, and the diffusion of the oxygen down the capillary is moderated by the bacteria's oxygen consumption, we switch the magnetic field direction and calculate the spatial distribution until a steady state is reached.

RESULTS

In this study, 12 diverse MTB strains were used to study magneto-aerotaxis. Although all the strains produce magnetite magnetosomes, their diversity is reflected in the variation of cell morphology, phylogeny, physiology, flagellar apparatus, and morphology of their magnetosomes (Table 1). Five strains (*Ms. gryphiswaldense* (14), *Magnetovibrio blakemorei* (15), *Magnetospira thiophila* (16), *Magnetococcus marinus* (17), and *Desulfovibrio magneticus* (18)) have already been thoroughly characterized (11). Three strains (UT-4 (19), LM-1 (19), and SS-5 (20)) have been partially described in the literature (4). The remaining four strains (PR-1, PR-2, PR-3, and SS-1) were recently isolated in axenic culture and have not been previously described (see Materials and Methods; Fig. S2 in the Supporting Material). All MTB were cultivated in semisolid, oxygen-gradient media (strain MSR-1 was in addition also cultivated in liquid medium), in the absence of any other potential terminal electron acceptors. Under these conditions, all the strains initially formed a microaerophilic band of cells at the OAI. When observed under a light microscope, under homogeneous, oxic conditions, all 12 MTB displayed a polar magnetotactic behavior (11), and were predominantly NS (Fig. S3). To work with homogenously polarized cells, NS cells were magnetically separated from SS cells, so only NS cells were present in subsequent experiments (Fig. S3). Magnetic separation was also used to transfer the cells into a liquid medium containing the oxygen-sensitive ruthenium fluorochrome (see Materials and Methods). Although NS and SS cells of the 12 MTB were successfully separated, some of the NS cells of *Magnetospira thiophila* strain MMS-1 spontaneously became SS as observed under the light microscope. It is possible that this polarity reversal is due to exposure to the light of the microscope. The cells that stayed at the North edge of the drop stopped moving after 1 min of observation (Fig. S3). This behavior is similar to the one described for a congeneric MTB *Magnetospira* sp. QH-2 (21).

All magnetotactic strains form a band at an oxygen concentration lower than 25 μM

The motile behavior of each strain was studied in a microcapillary sealed at one extremity using a petroleum jelly plug and placed in a magnetic field of 50 μT (strength of the Earth's field) oriented antiparallel to the oxygen gradient (position in Northern Hemisphere environments). Respiration by the cells and the oxygen diffusion from the open

end resulted in the formation of the oxygen gradient. Bacteria formed a microaerobic band 15 to 45 min after their transfer into the microcapillary. Once the band formed, cells continued to swim back and forth along **B** through the band. Once they reached the regions of too high or too low oxygen concentration, cells reversed their swimming direction without reorientation of the cell body (Movie S1). The distance traveled by the cells in the oxic or anoxic sides of the band was variable depending on the strains. For instance, strains MMS-1, LM-1, and the three magnetotactic cocci MC-1, PR-3, and SS-1, made long excursions around the band (Figs. 1 and S4). In contrast, cells of strains MSR-1 and PR-1 made short excursions in the region of too high or too low oxygen concentration (Figs. 1 and S4).

An oxygen-sensitive fluorescent probe (12) was used to measure the oxygen concentration along the microcapillary (Figs. 1 and S4). All MTB formed a well-defined band at an oxygen concentration in the microaerobic range (0–25 μM).

High-speed videos of bacteria swimming in the surrounding of the band were recorded and analyzed (Fig. 2 and Table S2). Using custom-written MATLAB code, swimming velocities of cells swimming away from and toward the center of the band were measured on the oxic and anoxic sides of the band. In the oxic region, all MTB except strain LM-1 had higher mean velocities when they swam toward the band than when they swam away from the band. For most MTB, there was no statistically significant difference of velocities on the anoxic side of the band (Fig. 2 and Table S2).

Six magneto-aerotactic behaviors were observed

In the microcapillary assay, all tested strains produced a microaerobic band of cells when the ambient magnetic field was pointed toward the anoxic zone, as in the Northern Hemisphere. To classify the different magnetotactic behaviors, we observed the effect of reversal of the ambient magnetic field on the cells in a stable microaerobic band (9). The change of magnetic field polarity induces a response from the cells that likely does not reflect an evolutionary adaptation. Thus, this experiment is not representative of the ecological context but is rather designed to extract information about the possible links between oxygen sensing mechanisms, alignment with the magnetic fields, and motility. In seven of the 12 strains (strains MC-1, PR-3, SS-1, MMS-1, PR-2, LM-1, and UT-4) (Fig. 3 *A*), the

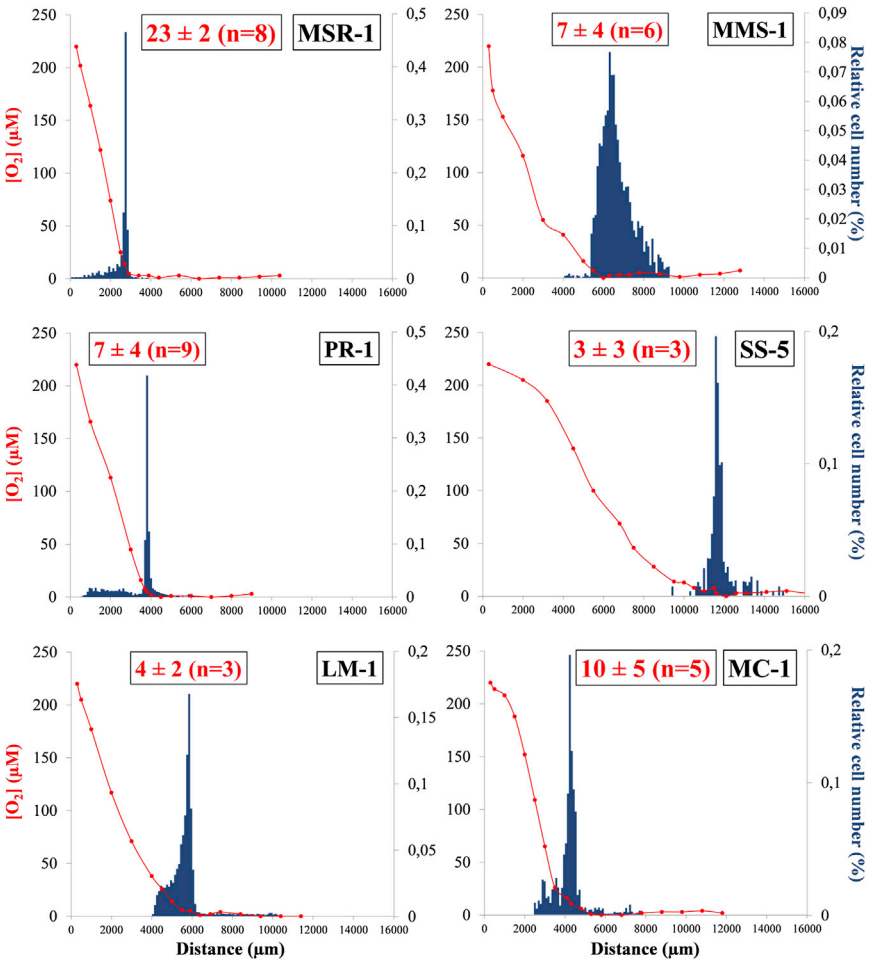

FIGURE 1 Relative cell distributions (*blue histograms*) of six of the 12 different magnetotactic bacteria under study in oxygen gradients (*red circles*). Each graph was made from a single microcapillary. Oxygen concentrations were obtained from one measurement at different positions along the capillary. In red is the value of the oxygen concentration (in μM) in the center of the aerotactic band (n represents the number of capillaries used to measure the average oxygen concentration at the band; see Materials and Methods for the error calculation). The relative number of cells were measured every 100 μm from triplicate counts. The same capillary was also used to measure the oxygen concentrations. For strain MSR-1, the distribution of cells were determined from a total of 3600 cells; for strain MMS-1 from 2166 cells; for strain PR-1 from 4391 cells; for strain SS-5 from 275 cells; for strain LM-1 from 11,754 cells; and for strain MC-1 from 1116 cells. To see this figure in color, go online.

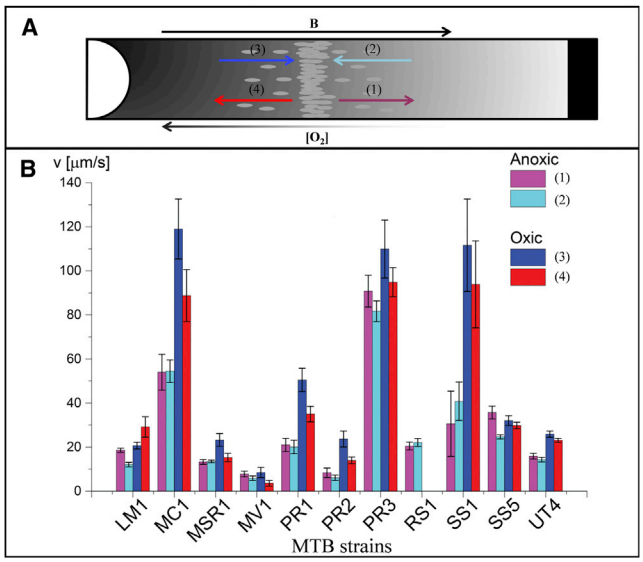

FIGURE 2 Speed motility (in $\mu m \times s^{-1}$) of the cells swimming in the anoxic or oxic zone surrounding the microaerotactic band. (*A*) Shows a representation of the different directions of motility that magnetotactic cells can have on the oxic and anoxic sides of a microaerobic band in a microcapillary exposed to a magnetic field (*B*) oriented antiparallel to the oxygen gradient. Cells are shown swimming from the band toward the anoxic zone (*purple*), from the anoxic zone toward the band (*light blue*), from the band toward the oxic zone (*red*), and from the oxic zone toward the band (*dark blue*). Histogram (*B*) and Table S2 show the average velocities of 11 MTB depending on their swimming direction and their position compared to the microaerotactic band. The swimming speed of strain MMS-1 could not be tracked due to its sensitivity of the light of the microscope. To see this figure in color, go online.

band split into two subbands, one moving toward the meniscus and one moving toward the closed, anoxic end of the capillary. This behavior, previously observed for strain MC-1, corresponds to the previously described polar magneto-aerotaxis (9).

When *Ms. gryphiswaldense* strain MSR-1 was grown in an oxygen gradient, the inversion of **B** resulted in the formation of three different subgroups (see Fig. 3 *C*). One of them stayed at its original position; after 1 h, this subgroup did not move significantly in the capillary. A second subgroup swam toward the oxic zone, whereas a third subgroup swam toward the anoxic zone. Thus, cells of strain MSR-1 behaved, under these conditions, as a mixture of polar and axial magnetotactic cells. The axial behavior, previously described for *Ms. magnetotacticum* (9), was observed only when *Ms. gryphiswaldense* was grown under a homogenous concentration of oxygen (Fig. 3 *B*).

For strain PR-1, two subgroups were observed. One subgroup remained at the original position of the band; 1 h after inversion of **B**, this subgroup of cells stayed at the same position. A second subgroup swam toward the oxic zone (Fig. 3 *D*). No cells swam toward the anoxic zone. Finally, cells of strains MV-1, SS-5, and RS-1 migrated as a single subgroup after inversion of **B**. For MV-1 and SS-5, all cells swam toward the oxic zone (Fig. 3 *E*), whereas cells of strain RS-1 swam toward the anoxic zone (Fig. 3 *F*). These results suggest that the actual model of magneto-aerotaxis is more complex than previously thought.

Three magneto-aerotactic mechanisms were observed in a model involving different sensing modes

Finally, we implemented different sensing mechanisms in a one-dimensional model for magneto-aerotaxis. This model is based on previous modeling work on aerotaxis (22) and magneto-aerotaxis (12,13). It describes swimming and reversals of the swimming direction, oxygen diffusion and oxygen consumption by the bacteria using three equations for oxygen concentration profiles, and for the densities of left-moving and right-moving cells (see Materials and Methods). The reversal rates are determined by the local oxygen concentration combined with either the magnetic field direction or the local oxygen gradient, depending on the assumed mechanism of sensing. Thus, in the model, migration of bacteria toward the band arises from a dependence of the reversal rates on the environmental conditions. In addition, the increased velocity when swimming toward the band (on the *oxic side*, Fig. 2) also contributes to such migration, but this effect was not included in the model described here.

In this model, the different magneto-aerotactic behaviors observed experimentally can be implemented as different sensing mechanisms. In all cases, cells have a low basal rate for reversals of their swimming direction, which is enhanced under certain conditions. A minimal implementation is based on step functions, in which the reversal rates attain one of two possible values, depending on the oxygen concentration and either the oxygen gradient or the magnetic field. The axial mechanism can be modeled with a reversal rate that depends on both the local oxygen gradient and the local oxygen concentration as follows: the reversal rate is increased when the bacterium either swims parallel to the oxygen gradient and the local oxygen concentration is above an upper threshold concentration (i.e., in the oxic zone) or when it swims antiparallel to the gradient with a local concentration below a lower threshold (in the anoxic zone). Sensing of the gradient likely arises from temporal comparison between consecutive measurements of the oxygen concentration while swimming. This is the scenario we have considered in our previous work (12). In this case, the magnetic field only constrains the motion to one dimension and does not directly affect sensing and decision-making.

For the polar mechanism, the reversal rates do not depend on the oxygen gradient, but rather on the magnetic field. In this case, the reversal rate is enhanced either when the oxygen concentration is above the upper threshold and swimming is antiparallel to the magnetic field, or when

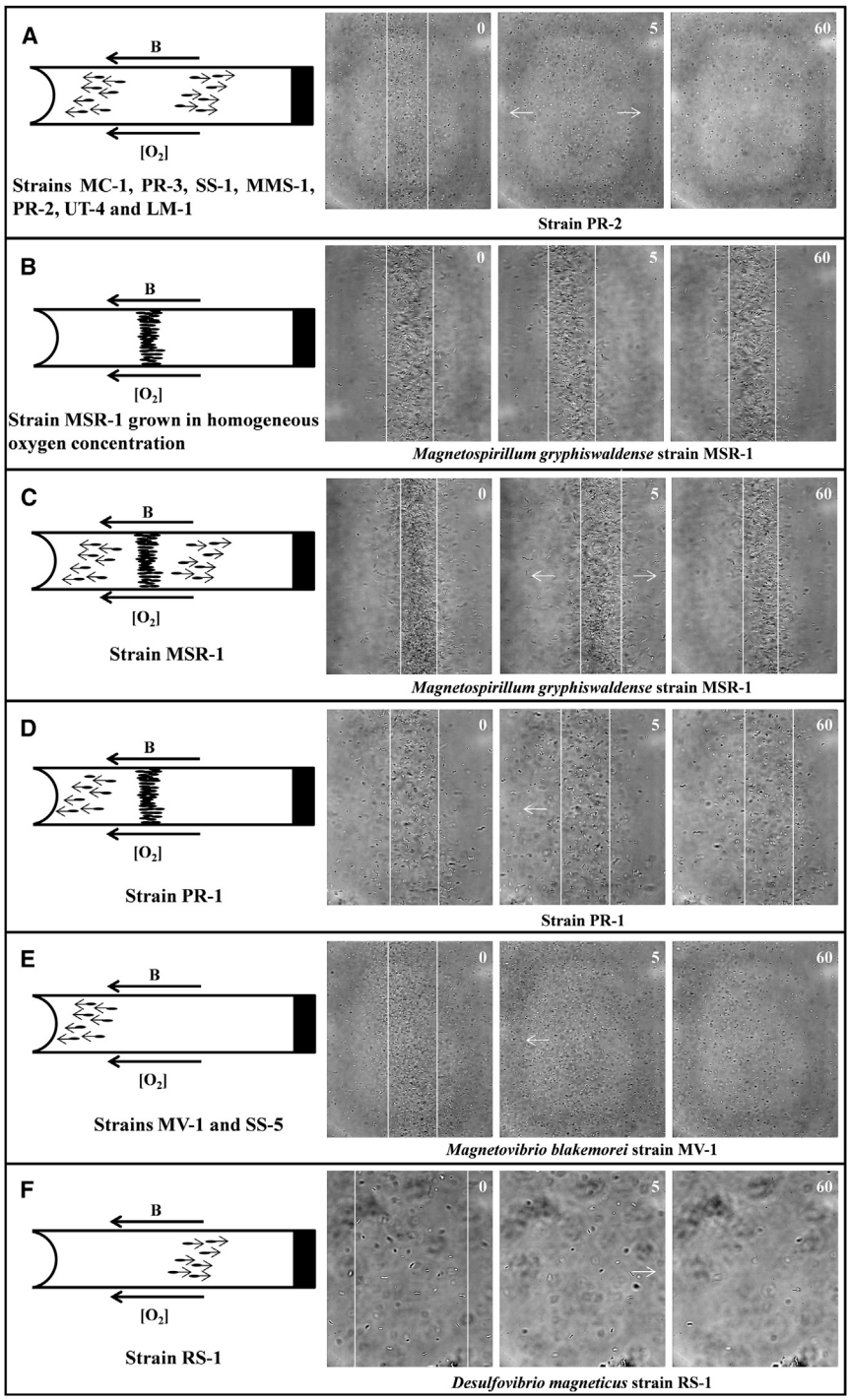

FIGURE 3 Six different behaviors are observed when the magnetic field (**B**) applied along a microcapillary containing a microaerotactic band of MTB is switched 180° to the initial direction. Each panel represents a drawing of the microcapillary followed by three light microscope pictures taken before the inversion of **B**, 5 s and 60 s after **B** was inversed. (*A*) Behavior observed for strains MC-1, PR-3, SS-1, MMS-1, PR-2, UT-4, and LM-1. Two different subgroups can be discerned when **B** is switched: 1), cells that are swimming parallel to **B** at the moment **B** is switched rotate 180° and swim toward the oxic zone; and 2), cells that are swimming antiparallel to **B** at the moment **B** is switched rotate 180° and swim toward the anoxic zone. (*B*) Behavior observed for *Ms. gryphiswaldense* strain MSR-1 grown in homogeneous-oxygen concentration. When **B** is switched cells rotate and continue to swim back and forth in the band. (*C*) Behavior observed for *Ms. gryphiswaldense* strain MSR-1 grown in semi-solid, oxygen gradient medium. Three different subgroups can be discerned when **B** is switched: 1), cells that rotate and stay in the band; 2), cells that are swimming parallel to **B** rotate and swim toward the oxic zone; and 3), cells that are swimming antiparallel to **B** rotate and swim toward the anoxic zone. (*D*) Strain PR-1 devolves into two subgroups when **B** is parallel to the oxygen gradient: 1), cells that rotate and continue to swim back and forth in the band; 2), cells that are swimming parallel and antiparallel to **B** rotate and swim toward the meniscus. (*E*) For strains MV-1 and SS-5, when **B** is switched, cells that are swimming parallel to **B** rotate and swim toward the meniscus, whereas the cells that are swimming antiparallel to **B** rotate and swim toward the anoxic zone until they reach the anoxic zone where they reverse their direction of motility without turning around and swim toward the meniscus. (*F*) For strain RS-1, when **B** is switched all cells swim toward the anoxic zone. The cells that were swimming toward the oxic zone rotate and swim toward the anoxic zone, whereas cells that were swimming toward the anoxic zone rotate and swim toward the meniscus until they reach a zone with a too high oxygen concentration where they reverse their direction of motility without turning around and swim toward the anoxic zone.

the oxygen concentration is below a lower threshold and the swimming direction is parallel to the field. This can be interpreted as the magnetic field providing the directional information that in the axial case is gained from sensing the oxygen gradient. The model of polar or axial magneto-aerotaxis proposed by Frankel et al. (9) arises as a limiting case from our description, when the bias toward the preferred direction of motion is very strong.

A third sensing mechanism is observed and does not fit with either the polar or axial ones. For this mechanism, which we name unipolar, the reversal rate is determined by the oxygen gradient in one of the two zones: oxic (unipolar behavior directed toward the oxic zone) or anoxic (unipolar behavior directed toward the anoxic zone), but the magnetic field in the other. For the unipolar behavior directed toward the anoxic side, the local oxygen gradient

is taken into account for reversal on the oxic side and the direction of the magnetic field on the anoxic side, and vice versa for unipolar behavior directed toward the oxic side. The previously described polar magneto-aerotactic behavior should then be named dipolar to be differentiated to the unipolar behavior described here. Both dipolar and unipolar mechanisms are displayed by bacteria that have a polar behavior, the former does not have a globally preferred polarity, whereas the latter has a preferred polarity either toward the oxic or anoxic zone (Table 1).

In each case, we simulated the establishment of the magneto-aerotactic band as well as the dynamics of the band after reversal of the field (Fig. 4, *B–E*). In all cases, a stationary band of cells formed within 30 min (after an initial movement of the band toward the oxic side) if the magnetic field was antiparallel to the oxygen gradient, indicating that the implementations of the different magneto-aerotactic mechanisms are equivalent when the field is antiparallel to the oxygen gradient. Upon reversal of the magnetic field (at time 30), the four mechanisms resulted in different behaviors, in agreement with experimental observations. Fig. 4 shows that the different implementations of sensing mechanisms indeed exhibited the expected behaviors of sensing seen in the experiments, which justifies using the same names for the different sensing modes.

The average position of the bacteria while the band is formed, and after the magnetic field reversal, is compared for different mechanisms and shown in Fig. S5.

DISCUSSION

Microaerotactic band formation

In this study, we addressed the magneto-aerotactic behavior of 12 cultured strains of different MTB in microcapillaries containing an oxygen gradient. A fluorescent dye-based technique was used to measure the oxygen concentration within the capillary. All strains formed aerotactic bands in the range of 0–25 μM O_2. These values correspond to those measured for microaerobic bands formed by microaerophilic, nonmagnetotactic bacteria such as *Azospirillum brasilense* (23), sulfide-oxidizing bacteria (24,25), or *Desulfovibrio vulgaris* Hildenborough (26).

By continuously swimming along the magnetic field, the cells make traversals between the oxic and anoxic sides of the band. The motility pattern can be described as a run and reverse pattern: cells approaching the borders of the band on the oxic or anoxic side stop and reverse direction by reversing the sense of their flagella rotation (25,27), i.e., the cells reverse swimming direction without turning

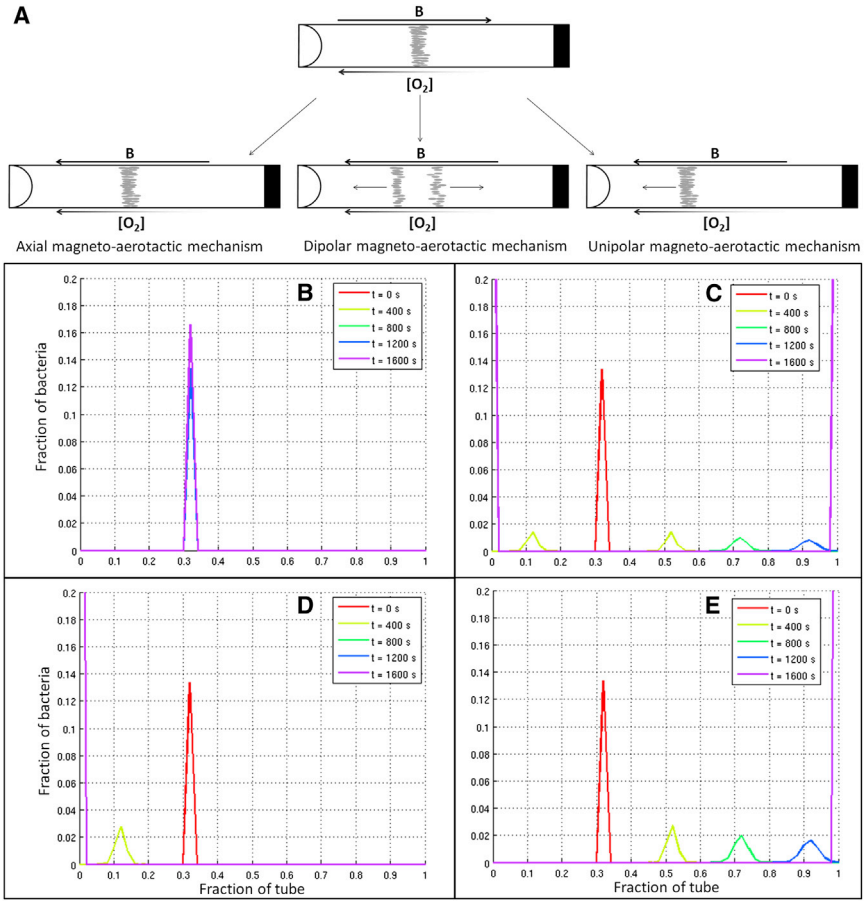

FIGURE 4 Model for the different magneto-aerotactic mechanisms. (*A*) Illustration of the three magneto-aerotactic mechanisms displayed by the magnetotactic bacteria when the magnetic field **B** is rotated 180° from antiparallel (position in Northern Hemisphere environments) to parallel to the oxygen gradient. The unipolar model represented here corresponds to the unipolar magneto-aerotactic mechanism directed toward the oxic zone. (*B–E*) One-dimensional model for the different magneto-aerotactic mechanisms: axial, dipolar, and unipolar (directed toward the oxic zone (*D*) and directed toward the anoxic zone (*E*)), respectively. To see this figure in color, go online.

around. The same behavior was observed for the 12 microaerophilic MTB under study. This chemotactic strategy resembles the strategy described in marine bacteria (25) and is different from the run and tumble strategy described in *Escherichia coli* (28).

In our strains, swimming speeds were generally higher on the oxic side than on the anoxic side. On the anoxic side of the band, cells swim away from the center of the band as fast as those moving toward the center. On the oxic side, cells move toward the center faster than those moving away from the center of the band. This observation corresponds to previous observations for axial cells of strain MSR-1 (12). It is consistent with the fact that the proton motive force is the source of energy driving flagellar motors in bacteria (27,29) and is dependent on oxygen concentration for microaerophilic cells (23). Thus, it is likely that microaerophilic cells in the oxic zone swim faster due to the higher amount of energy available for the flagellar motors in this zone. Within the oxic zone the proton motive force would be lower in the cells moving away from the center of the band than for those that are moving toward the center of the band.

The long excursions performed by *Magnetococcus marinus* strain MC-1 above and below the center of the microaerotactic band were previously explained as a way for cells to increase their access to energy by successively swimming to higher concentrations of their electron source (reduced sulfur) and electron acceptor (9) (Fig. 1), as opposed to remaining in the low concentrations of energy source and electron acceptor close to the center of the band. The magnetotactic coccus SS-1, as well as the marine spirillum *Magnetospira thiophila* strain MMS-1, two sulfide-oxidizing bacteria, also display this behavior. Another magnetic coccus, strain PR-3, closely related to MC-1, grows with organic sources of energy (see the Supporting Material) instead of reduced sulfur and also displays this behavior (Fig. 1). Thus, the long excursions by these MTB into the oxic and anoxic zones are not specifically connected with reduced sulfur metabolism. This might be a strategy by which small, fast-swimming cells increase the time they spend at the higher concentration of energy sources to offset the effect of low surface area on the uptake of the electron source.

MTB isolated in axenic culture so far typically form a microaerotactic band in an oxygen gradient biotope, including the sulfate-reducing organisms such as *Desulfovibrio magneticus* strain RS-1, strain FH-1 (30), and the alkaliphilic strains ML-1 and AV-1 (31). This proves that all MTB, even those that are facultative anaerobes, take advantage of magnetotaxis depending on the nutrient availability in the environment. Only one magnetotactic bacterium recently isolated in culture, *Candidatus* Desulfamplus magnetomortis strain BW-1 (32), does not form a microaerotactic band when grown in an oxygen-gradient medium, but rather form aggregates below the oxic-anoxic transition zone.

Relevance of axial magnetotaxis

Magnetospirillum species have usually been classified as displaying axial magnetotaxis, based on observations of *Ms. magnetotacticum* (9,10). Nevertheless, contrary to that classification, it was previously reported that freshly isolated *Magnetospirillum* species have a preferred swimming polarity when isolated from their natural habitat (10,19,33), suggesting that these cells use a dipolar magneto-aerotactic mechanisms. In this study, we found different magnetotactic behaviors for *Ms. gryphiswaldense* MSR-1 grown under different conditions, with axial behavior for MSR-1 grown under a homogeneous-oxygen concentration and a mixture of dipolar and axial behaviors for cells grown in an oxygen gradient (Fig. 3, *B* and *C*). Thus, axial magnetotaxis could be a behavior caused by the repeated growth of MTB in culture media containing an homogenous concentration of oxygen (e.g., 1% (9)) and an adaptation of the cells to an artificial growth condition. Thus, the magneto-aerotactic behavior of *Magnetospirillum* appears to be regulated by physiological and environmental conditions. It does not rule out the possibility that some species of MTB in the environment do not display a preferred pole of motility and use the magnetic field only as an axis of motility because it was shown that such behavior was efficient to find the OAI (9). However, it would be necessary to observe the sample containing MTB without a previous step of magnetic concentration that automatically selects bacteria that have a preferred polarity.

Sensing mechanisms responsible for magneto-aerotaxis

Because nonmagnetotactic aerotactic bacteria are not readily constrained by the ambient magnetic field they can reorient to reach their favorite niche, their oxygen sensors cannot be artificially placed in the wrong position with respect to the oxygen gradient. MTB can be used to study this unnatural state because their orientation can be directed at will using low intensity magnetic fields.

The responses of cells in the microaerotactic bands to reversal of the magnetic field reveal six different magneto-aerotactic behaviors explained by three different mechanisms: axial, dipolar (9) and, a previously undescribed mechanism, unipolar magneto-aerotaxis (Fig. 4). Notably, no obvious correlation of these behaviors with the physiology, phylogeny, morphology, speed of motility, or flagellar apparatus of the strains could be observed (Table 1). Nevertheless, the unipolar mechanism appears to occur only in bacteria having one polar flagellum, whereas the axial mechanism was observed only in bacteria with two polar flagella (Table 1). However, some magnetotactic spirilla such as MMS-1 and UT-4 have two polar flagella (Table 1), yet exhibit dipolar magnetotaxis, indicating that magnetotactic spirilla do not necessarily exhibit axial magnetotaxis.

The observed diversity of behaviors suggests that aerotaxis may be regulated differently in the different magnetotactic strains.

Reversing the magnetic field can be interpreted as giving magneto-aerotactic cells conflicting information, because in the natural habitat, the oxygen gradient and the magnetic field direction, that point in the opposite direction in the Northern Hemisphere, usually both direct the cells toward the microaerobic zone. Upon reversal of the field, however, the oxygen gradient directs their movements in one direction, whereas the magnetic field directs them in the opposite direction.

In axial magneto-aerotaxis (Figs. 3 *B* and 4 *B*), all cells in the band rotate by 180° when the field is reversed and the band stays intact in the same location. Thus, for these cells aerotaxis is prioritized over magnetotaxis, which also means that they must behave as if the cells were sensing the oxygen gradient whatever their orientation in the oxygen gradient. In addition, they must also distinguish whether the present oxygen concentration is above or below their preferred oxygen concentration to direct their motility up or down within the oxygen gradient.

In dipolar magneto-aerotaxis (Figs. 3 *A* and 4 *C*), inversion of the field also leads to rotation of the cells by 180°, but the band splits into two subgroups: one swims persistently antiparallel to the magnetic field all the way to the end of the anoxic zone; the other swims persistently parallel to the magnetic field all the way to the end of the oxic zone, at the meniscus. Therefore, these cells either cannot remember previous oxygen concentration measurements when presented with conflicting directional information, or they give priority to following the direction indicated by the magnetic field, for example by switching off their sensing mechanism for the oxygen under conditions of conflicting signals. A simple interpretation of the dipolar behavior is that the cells behave as though they are sensing the oxygen gradient (by sensing the oxygen concentration with a memory and comparing two consecutive measurements) only when the oxygen gradient is pointing in the opposite direction of the magnetic field for north-seeking MTB. In nonnatural conditions, dipolar cells would have their oxygen sensing mechanism turned off and would rely only on the magnetic field to direct their motility. When the anoxic end of the capillary is opened to allow oxygen diffusion and the formation of another OAI (with a gradient opposite to the one at the other extremity), the Northern Hemisphere orientation of the magnetic field and the oxygen gradient is restored at that end and cells that are swimming toward the anoxic zone reach this OAI and form an aerotactic band.

In unipolar magneto-aerotaxis (Figs. 3, *E* and *F*, and 4, *D* and *E*), the cells rotate by 180° with an inversion of the field, stay together and swim as a band either into the anoxic zone or into the oxic zone. This mechanism, observed for strains MV-1, SS-5, and RS-1, likely indicates that two distinct sensing mechanisms determine the overall swimming direction under oxic and anoxic conditions (above and below the preferred microoxic zone) in these strains (and potentially in others as well). The unidirectional behavior can be explained by our model (Fig. 4) if we assume that the cells can behave as sensing the oxygen gradient under either oxic or anoxic conditions, but follow the magnetic field under the other condition. Strains MV-1 and SS-5 display a unipolar magneto-aerotaxis directed toward the oxic zone: cells that were swimming parallel to **B** rotate by 180° with the inversion of the field, and swim all the way toward the oxic zone, whereas cells that were swimming antiparallel to **B** also rotate by 180° with the inversion of the field, swim until they reach a zone that can be considered as too low in oxygen where they switch their swimming direction without turning around, and swim all the way toward the oxic zone. The same behavior was observed for strain RS-1 but all cells swam toward the anoxic zone after inversion of the field. One can speculate that this is more favorable to RS-1 for a sulfate-reducing bacterium for which the anoxic side is likely less toxic than the oxic side due to a greater sensitivity to oxygen.

Coexistence of different sensing mechanisms in one strain

Cells of strain MSR-1 grown in an oxygen-gradient medium, exhibit a combination of two mechanisms (Fig. 3 *C*), dipolar and axial (likewise strain PR-1 combines unipolar magneto-aerotaxis directed toward the oxic zone and axial magnetotaxis, Fig. 3 *D*). These combinations likely reflect mixed populations, but it is unclear why two distinct subpopulations exist in one strain. From the point of view of sensing mechanisms, the coexistence of these two populations suggests that although these cells behave like having the ability to sense the oxygen gradient, not all cells in the population make use of it. It is possible that the observed behavior depends on the history of the individual cell, for example if some of the cells in the microaerophilic band were exposed to a homogeneous concentration of oxygen long enough to become axial. This scenario would indeed be most likely with strains MSR-1 and PR-1, which in this type of medium tend to form thick bands that diffuse in the oxic zone. One may also speculate whether the heterogeneous behavior in these populations is a case of bet-hedging (34), where the population deals with the conflicting directional signals from the magnetic field and the oxygen gradient by splitting into two subpopulations following one or the other. Following different individual courses of action could represent an advantage in fluctuating environments. The presence of a large number of chemotaxis proteins in species of the *Magnetospirillum* genus (e.g., 65 in strain MS-1 (35) and 64 in strain AMB-1 (36)) could also explain the different magnetotactic

behaviors with their expression only under certain growth conditions.

Putative molecular background

Understanding the molecular mechanisms of oxygen sensing would likely allow us to obtain a more mechanistic understanding of the different magneto-aerotactic behaviors. In general, chemotactic sensors are responsible for sensing the oxygen concentration (37). The major players in chemotaxis signal transduction pathway are the transmembrane methyl-accepting chemotaxis protein (MCP) receptors and cytosolic proteins (Che). Typically, chemotactic gradient sensing in bacteria is based on temporal comparison of local concentrations during swimming. In this way, increasing the distance over which a gradient is sensed and thus the concentration difference are increased, boosting the latter beyond fundamental limits imposed by noise (37–39). However, spatial gradient sensing with receptors at both ends of the cell has also been proposed for some vibrioid bacteria in sulfidic marine sediment (24). Although unconventional and somewhat speculative, spatial gradient sensing is an attractive hypothesis in aerotaxis, because the observation that most of the nonmagnetotactic microaerophilic bacteria observed in microcapillaries do not rotate when reversing their direction of motion (i.e., they change the direction of motility by changing the sense of their flagellar rotation rather than by a U-turn). This suggests that the orientation of the cell compared to the gradient may be important, for example as a consequence of the polarization of the chemotactic sensors in the cell. In the case of MTB, the reversal of the magnetic field reorients the cells and thus the different magneto-aerotactic behaviors we observe may reflect whether the correct orientation of the chemotactic system is indeed required in different bacteria.

Our observation of the unipolar behavior suggests that there are two distinct sensory systems for low and high oxygen concentrations, but the identity of the sensors and their molecular mechanisms remain to be resolved. Oxygen sensors known in *E. coli* include the oxygen transducers Aer and Tsr, which sense the change in electron transport by sensing a change in redox potential, proton motive force, or possibly electron flux. They are related to methyl-accepting proteins (MCP) that transfer a signal to the flagellar motor to control its sense of rotation (37,40–42). However, even in *E. coli* their precise sensory mechanisms remain to be resolved (43). Homologs of Aer and Tsr proteins, with HAMP and/or PAS domains similar than those described in *E. coli*, can be found in MTB with their genome sequenced (e.g., Aer-like for the strains MSR-1: CAM75681, SS-5: KJ433374, and MC-1: YP_866298; Tsr-like for the strains SS-5: KJ433375, MSR-1: CAM75482, and MC-1: YP_867203). These proteins could be the sensors at the origin of the different magneto-aerotactic mechanisms described here.

Potential use of MTB as model organisms to study tactic behaviors

We observed six different magneto-aerotactic behaviors. This points toward different aerotaxis regulation in the different magnetotactic strains, which could also be true for nonmagnetotactic microorganisms, although this hypothesis might be difficult to test. MTB might thus be promising model organisms to understand the mechanisms responsible for aerotaxis. In particular, magnetotactic cells can be magnetically directed in an oxygen gradient to understand the role of the position of the chemotactic sensors that present a polarization and which orientation presents an importance in their functioning.

In addition, the mechanisms from other types of taxis could also be resolved using MTB as models. For instance, magnetotactic cells would be a very interesting model to study klinotaxis, a taxis based on temporal gradient sensing (24).

ACCESSION NUMBERS

Accession numbers of the putative Tsr and Aer genes of strain SS-5 are KJ433374 and KJ433375, respectively. The 16S rRNA gene sequences of SS-1, PR-1, PR-2, and PR-3 carry accession numbers JN896752, KJ442651, KJ44262, KJ442653, respectively.

SUPPORTING MATERIAL

Supporting Materials and Methods, six figures, two tables, and one movie are available at http://www.biophysj.org/biophysj/supplemental/S0006-3495(14)00623-7.

We thank G. Adryanczyk for her help in the phylogenetic identification of the newly isolated magnetotactic strains.

The research was supported by the Max Planck Society and the European Research Council through a Starting Grant to D.F. (grant No. 256915-MB2). L.L. is supported by the International Max Planck Research School (IMPRS) on Multiscale Bio-Systems. D.F. and S.K. acknowledge financial support from the Deutsche Forschungsgemeinschaft within the framework of the Priority Programm 1726 “Microswimmers – from single particle motion to collective behavior” (grant No. FA 835/7-1 and KL 818/2-1).

REFERENCES

1. Brune, A., P. Frenzel, and H. Cypionka. 2000. Life at the oxic-anoxic interface: microbial activities and adaptations. *FEMS Microbiol. Rev.* 24:691–710.
2. Fenchel, T. 1994. Motility and chemosensory behavior of the sulfur bacterium *Thiovulum majus*. *Microbiol.-UK.* 140:3109–3116.
3. Blakemore, R. 1975. Magnetotactic bacteria. *Science.* 190:377–379.
4. Lefèvre, C. T., and D. A. Bazylinski. 2013. Ecology, diversity, and evolution of magnetotactic bacteria. *Microbiol. Mol. Biol. Rev.* 77: 497–526.
5. Faivre, D., and D. Schüler. 2008. Magnetotactic bacteria and magnetosomes. *Chem. Rev.* 108:4875–4898.
6. Komeili, A. 2012. Molecular mechanisms of compartmentalization and biomineralization in magnetotactic bacteria. *FEMS Microbiol. Rev.* 36:232–255.

7. Bazylinski, D. A., R. B. Frankel, …, A. K. Hanson. 1995. Controlled biomineralization of magnetite (Fe(inf3)O(inf4)) and greigite (Fe(inf3)S(inf4)) in a magnetotactic bacterium. *Appl. Environ. Microbiol.* 61:3232–3239.
8. Blakemore, R. P., R. B. Frankel, and A. J. Kalmijn. 1980. South-seeking magnetotactic bacteria in the southern-hemisphere. *Nature.* 286:384–385.
9. Frankel, R. B., D. A. Bazylinski, …, B. L. Taylor. 1997. Magneto-aerotaxis in marine coccoid bacteria. *Biophys. J.* 73:994–1000.
10. Frankel, R. B., T. J. Williams, and D. A. Bazylinski. 2007. Magneto-aerotaxis. *In* Magnetoreception and Magnetosomes in Bacteria. D. Schüler, editor. Springer, Berlin/Heidelberg, pp. 1–24.
11. Bazylinski, D. A., C. T. Lefèvre, and D. Schüler. 2013. Magnetotactic bacteria. *In* The Prokaryotes. E. Rosenberg, E. F. DeLong, S. Lory, E. Stackebrandt, and F. Thompson, editors. Springer, Berlin Heidelberg, pp. 453–494.
12. Bennet, M., A. McCarthy, F. Dmitri, M. R. Edwards, …, F. Repp. 2014. A microscopy platform for correlative studies of tactic behaviors of microorganisms. *PLoS One.* Published online January 31, 2014. http//dx.doi.org/10.1371/journal.pone.0101150.
13. Smith, M. J., P. E. Sheehan, …, L. J. Whitman. 2006. Quantifying the magnetic advantage in magnetotaxis. *Biophys. J.* 91:1098–1107.
14. Schleifer, K. H., D. Schüler, …, M. Kohler. 1991. The genus *Magnetospirillum* gen. nov. description of *Magnetospirillum gryphiswaldense* sp. nov. and transfer of *Aquaspirillum magnetotacticum* to *Magnetospirillum magnetotacticum* comb. nov. *Syst. Appl. Microbiol.* 14:379–385.
15. Bazylinski, D. A., T. J. Williams, …, B. Simpson. 2013. *Magnetovibrio blakemorei* gen. nov., sp. nov., a magnetotactic bacterium (Alphaproteobacteria: Rhodospirillaceae) isolated from a salt marsh. *Int. J. Syst. Evol. Microbiol.* 63:1824–1833.
16. Williams, T. J., C. T. Lefèvre, …, D. A. Bazylinski. 2012. *Magnetospira thiophila* gen. nov., sp. nov., a marine magnetotactic bacterium that represents a novel lineage within the Rhodospirillaceae (Alphaproteobacteria). *Int. J. Syst. Evol. Microbiol.* 62:2443–2450.
17. Bazylinski, D. A., T. J. Williams, …, T. J. Beveridge. 2013. *Magnetococcus marinus* gen. nov., sp. nov., a marine, magnetotactic bacterium that represents a novel lineage (Magnetococcaceae fam. nov., Magnetococcales ord. nov.) at the base of the Alphaproteobacteria. *Int. J. Syst. Evol. Microbiol.* 63:801–808.
18. Sakaguchi, T., A. Arakaki, and T. Matsunaga. 2002. *Desulfovibrio magneticus* sp. nov., a novel sulfate-reducing bacterium that produces intracellular single-domain-sized magnetite particles. *Int. J. Syst. Evol. Microbiol.* 52:215–221.
19. Lefèvre, C. T., M. L. Schmidt, …, D. A. Bazylinski. 2012. Insight into the evolution of magnetotaxis in *Magnetospirillum* spp., based on *mam* gene phylogeny. *Appl. Environ. Microbiol.* 78:7238–7248.
20. Lefèvre, C. T., N. Viloria, …, D. A. Bazylinski. 2012. Novel magnetite-producing magnetotactic bacteria belonging to the Gammaproteobacteria. *ISME J.* 6:440–450.
21. Zhu, K., H. Pan, …, L. F. Wu. 2010. Isolation and characterization of a marine magnetotactic spirillum axenic culture QH-2 from an intertidal zone of the China Sea. *Res. Microbiol.* 161:276–283.
22. Mazzag, B. C., I. B. Zhulin, and A. Mogilner. 2003. Model of bacterial band formation in aerotaxis. *Biophys. J.* 85:3558–3574.
23. Zhulin, I. B., V. A. Bespalov, …, B. L. Taylor. 1996. Oxygen taxis and proton motive force in *Azospirillum brasilense*. *J. Bacteriol.* 178:5199–5204.
24. Thar, R., and M. Kuhl. 2003. Bacteria are not too small for spatial sensing of chemical gradients: an experimental evidence. *Proc. Natl. Acad. Sci. USA.* 100:5748–5753.
25. Thar, R., and T. Fenchel. 2005. Survey of motile microaerophilic bacterial morphotypes in the oxygen gradient above a marine sulfidic sediment. *Appl. Environ. Microbiol.* 71:3682–3691.
26. Johnson, M. S., I. B. Zhulin, …, B. L. Taylor. 1997. Oxygen-dependent growth of the obligate anaerobe *Desulfovibrio vulgaris* Hildenborough. *J. Bacteriol.* 179:5598–5601.
27. Larsen, S. H., J. Adler, …, R. W. Hogg. 1974. Chemomechanical coupling without ATP: the source of energy for motility and chemotaxis in bacteria. *Proc. Natl. Acad. Sci. USA.* 71:1239–1243.
28. Berg, H. C., and D. A. Brown. 1972. Chemotaxis in *Escherichia coli* analyzed by three-dimensional tracking. *Nature.* 239:500–504.
29. Manson, M. D., P. Tedesco, …, C. Van der Drift. 1977. A proton motive force drives bacterial flagella. *Proc. Natl. Acad. Sci. USA.* 74:3060–3064.
30. Lefèvre, C. T., D. Trubitsyn, …, N. Ginet. 2013. Comparative genomic analysis of magnetotactic bacteria from the Deltaproteobacteria provides new insights into magnetite and greigite magnetosome genes required for magnetotaxis. *Environ. Microbiol.* 15:2712–2735.
31. Lefèvre, C. T., R. B. Frankel, …, D. A. Bazylinski. 2011. Isolation of obligately alkaliphilic magnetotactic bacteria from extremely alkaline environments. *Environ. Microbiol.* 13:2342–2350.
32. Lefèvre, C. T., N. Menguy, …, D. A. Bazylinski. 2011. A cultured greigite-producing magnetotactic bacterium in a novel group of sulfate-reducing bacteria. *Science.* 334:1720–1723.
33. Schüler, D., S. Spring, and D. A. Bazylinski. 1999. Improved technique for the isolation of magnetotactic spirilla from a freshwater sediment and their phylogenetic characterization. *Syst. Appl. Microbiol.* 22: 466–471.
34. Veening, J.-W., E. J. Stewart, …, L. W. Hamoen. 2008. Bet-hedging and epigenetic inheritance in bacterial cell development. *Proc. Natl. Acad. Sci. USA.* 105:4393–4398.
35. Alexandre, G., S. Greer-Phillips, and I. B. Zhulin. 2004. Ecological role of energy taxis in microorganisms. *FEMS Microbiol. Rev.* 28: 113–126.
36. Matsunaga, T., Y. Okamura, …, H. Takeyama. 2005. Complete genome sequence of the facultative anaerobic magnetotactic bacterium *Magnetospirillum* sp. strain AMB-1. *DNA Res.* 12:157–166.
37. Wadhams, G. H., and J. P. Armitage. 2004. Making sense of it all: bacterial chemotaxis. *Nat. Rev. Mol. Cell Biol.* 5:1024–1037.
38. Sourjik, V., and H. C. Berg. 2004. Functional interactions between receptors in bacterial chemotaxis. *Nature.* 428:437–441.
39. Sourjik, V., and N. S. Wingreen. 2012. Responding to chemical gradients: bacterial chemotaxis. *Curr. Opin. Cell Biol.* 24:262–268.
40. Edwards, J. C., M. S. Johnson, and B. L. Taylor. 2006. Differentiation between electron transport sensing and proton motive force sensing by the Aer and Tsr receptors for aerotaxis. *Mol. Microbiol.* 62:823–837.
41. Rebbapragada, A., M. S. Johnson, …, B. L. Taylor. 1997. The Aer protein and the serine chemoreceptor Tsr independently sense intracellular energy levels and transduce oxygen, redox, and energy signals for Escherichia coli behavior. *Proc. Natl. Acad. Sci. USA.* 94:10541–10546.
42. Bibikov, S. I., R. Biran, …, J. S. Parkinson. 1997. A signal transducer for aerotaxis in *Escherichia coli*. *J. Bacteriol.* 179:4075–4079.
43. Taylor, B. L. 2007. Aer on the inside looking out: paradigm for a PAS-HAMP role in sensing oxygen, redox and energy. *Mol. Microbiol.* 65:1415–1424.

Diversity of Magneto-Aerotactic Behaviors and Oxygen Sensing Mechanisms in Cultured Magnetotactic Bacteria

Christopher T. Lefèvre, Mathieu Bennet, Livnat Landau, Peter Vach, David Pignol, Dennis A. Bazylinski, Richard B. Frankel, Stefan Klumpp, and Damien Faivre

Supporting Material

MATERIALS AND METHODS

Isolation and growth of magnetotactic bacteria

Strains MSR-1, UT-4 and LM-1 were grown in the same freshwater medium in heterotrophic conditions. 5 ml of modified Wolfe's mineral elixir (1, 2), 0.2 ml 1% aqueous resazurin, 0.4 g NaCl, 0.3 g NH_4Cl, 0.1 g $MgSO_4$ • 7H2O, 0.05 g $CaCl_2$ • 2H2O, 1 g sodium succinate, 0.5 g sodium acetate and 0.2 g yeast extract (Difco Laboratories, Detroit, MI) were added to a liter of water, and the pH was adjusted to 7.0. A total of 1.6 g of Bacto agar (Difco Laboratories, Detroit, MI) was then added, after which the medium was autoclaved.

Strain RS-1 was grown in a freshwater medium in heterotrophic conditions. 5 ml of modified Wolfe's mineral elixir (1, 2) without sulfate, 0.2 ml 1% aqueous resazurin, 0.17 g $NaNO_3$, 0.082 $MgCl_2$ • $6H_2O$, 0.75 g sodium succinate and 0.25 g yeast extract. (Difco Laboratories, Detroit, MI) were added to a liter of water, and the pH was adjusted to 7.0. A total of 1.6 g of Bacto agar (Difco Laboratories, Detroit, MI) was then added, after which the medium was autoclaved.

Strains MV-1, PR-1, PR-2 and PR-3 were grown in the same saline medium in heterotrophic conditions. The formula of the artificial seawater was (per liter): 20 g NaCl, 6 g $MgCl_2$ • $6H_2O$, 3.24 g Na_2SO_4, 1 g $CaCl_2$ • $2H_2O$ and 0.5 g KCl. To a liter of this mixture, 5 ml of modified Wolfe's mineral elixir (1, 2), 0.2 ml 1% aqueous resazurin, 0.3 g NH_4Cl, 1 g sodium succinate, 2.4 g HEPES and 0.2 g yeast extract (Difco Laboratories, Detroit, MI) were added, and the pH was adjusted to 7.0. A total of 1.6 g of Bacto agar (Difco Laboratories, Detroit, MI) was then added, after which the medium was autoclaved.

Strains MC-1 and MMS-1 were grown in the same saline medium in autotrophic conditions. The formula of the artificial sea water was (per liter): 16.4 g NaCl, 3.5 g $MgCl_2 \cdot 6H_2O$, 2.8 g Na_2SO_4, 1 g $CaCl_2 \cdot 2H_2O$ and 0.5 g KCl. To a liter of this mixture, 5 ml of modified Wolfe's mineral elixir (1, 2), 0.2 ml 1% aqueous resazurin, 0.3 g NH_4Cl and 2.4 g HEPES were added, and the pH was adjusted to 7.0. A total of 1.6 g of Bacto agar (Difco Laboratories, Detroit, MI) was then added, after which the medium was autoclaved.

Strains SS-5 and SS-1 were grown in hypersaline media in autotrophic conditions using thiosulfate and sulfide, respectively as reduced sulfur compounds. The formula of the artificial seawater was (per liter): 37.8 g NaCl, 6 g $MgCl_2 \cdot 6H_2O$, 3.24 g Na_2SO_4, 0.5 g $CaCl_2 \cdot 2H_2O$ and 0.9 g KCl. To a liter of this mixture, 5 ml of modified Wolfe's mineral elixir (1, 2), 0.2 ml 1% aqueous resazurin and 0.3 g NH_4Cl were added, and the pH was adjusted to 7.0. A total of 1.6 g of Bacto agar (Difco Laboratories, Detroit, MI) was then added, after which the medium was autoclaved.

After autoclaving, the following ingredients were added as sterile stock solutions (per liter) in the five media described above: 0.5 ml of vitamin solution (3), 2.8 ml of 0.5 M $KHPO_4$ buffer (pH 7.0), 3 ml of 10 mM $FeCl_2 \cdot 4H_2O$ (in 0.02 N HCl), 1.8 ml of 0.8 M sodium bicarbonate ($NaHCO_3$) solution and 10 ml of a filter-sterilized, freshly made, 4% neutralized cysteine • HCl • 2H2O solution. In the medium of strains MC-1, MMS-1 and SS-5, 3 ml of 40% sodium thiosulfate ($Na_2S_2O_3 \cdot 5H_2O$) was added while the medium of strains SS-1 was supplemented with 5 ml of neutralized 100 mM sodium sulfide ($Na_2S \cdot 9H_2O$). The media were then dispensed into sterile, screw-cap glass tubes at ~80% of their volume and incubated at room temperature for several hours to solidify and to allow the oxygen gradient to form, as evidenced by the presence of a pink (oxidized) zone near the surface and a colorless (reduced) zone in the lower portion of the tubes due to the redox indicator resazurin.

Strains PR-1, PR-2 and PR-3 were isolated from samples collected from the same site at the Pointe Rouge Marina in Marseille, France. Strain SS-1 was isolated from sample collected at Salton Sea, California. Samples contained sediment together with the interface seawater, with a ratio of 1:2. Magnetotactic cells were magnetically concentrated by placing the south pole of a magnetic stirring bar next to sample bottles at the sediment–water interface for ~30 min, and then further purified using the capillary magnetic racetrack technique (4). Cells were used as inocula in semisolid, oxygen-gradient, enrichment media described above. Axenic cultures were obtained by dilution to extinction three times in succession in semisolid growth media.

Determination of 16S rRNA and phylogenetic analysis

16S rRNA genes were amplified using bacteria specific primers 27F 5'-AGAGTTTGATCMTGGCTCAG-3' and 1492R 5'-TACGGHTACCTTGTTACGACTT-3' (5). PCR products were cloned into pGEM-T Easy Vector (Promega Corporation, MadisonWI, USA) and sequenced (GATC Biotech AG, Germany). Alignment of 16S rRNA was performed using CLUSTAL W multiple alignment accessory application in the BioEdit sequence alignment editor (6). Phylogenetic trees were constructed using MEGA version 5 (7) applying the neighbor-joining method (8). Bootstrap values were calculated with 100 replicates.

Aggregate formation

About one hour after the transfer of the MTB in the capillary, a low proportion of cells stops swimming and aggregates in the band at the oxic-anoxic interface. These aggregates were

observed for almost all species throughout the entire depth of the capillary (Fig. S5). This behavior is likely due to the attachments of the cells to the walls of the capillary or to each other through the contact of their flagella or pili, as previously reported for *Magnetococcus marinus* (3).

REFERENCES

1. Wolin, E.A., M.J. Wolin, and R.S. Wolfe. 1963. Formation of methane by bacterial extracts. J. Biol. Chem. 238: 2882–2886.

2. Bazylinski, D.A., A.J. Dean, D. Schüler, E.J. Phillips, and D.R. Lovley. 2000. N2-dependent growth and nitrogenase activity in the metal-metabolizing bacteria, *Geobacter* and *Magnetospirillum* species. Environ. Microbiol. 2: 266–273.

3. Frankel, R.B., D.A. Bazylinski, M.S. Johnson, and B.L. Taylor. 1997. Magneto-aerotaxis in marine coccoid bacteria. Biophys. J. 73: 994–1000.

4. Wolfe, R.S., R.K. Thauer, and N. Pfennig. 1987. A “capillary racetrack” method for isolation of magnetotactic bacteria. FEMS Microbiol. Lett. 45: 31–35.

5. Lane, D.J. 1991. 16S/23S sequencing. In: Stackebrandt E, M Goodfellow, editors. Nucleic acid techniques in bacterial systematics. John Wiley & Sons: New York. pp. 115–175.

6. Hall, T. 1999. BioEdit: a user-friendly biological sequence alignment editor and analysis program for Windows 95/98/NT. Nucleic Acids Symp. Ser. 41: 95–98.

7. Tamura, K., D. Peterson, N. Peterson, G. Stecher, M. Nei, et al. 2011. MEGA5: molecular evolutionary genetics analysis using maximum likelihood, evolutionary distance, and maximum parsimony methods. Mol. Biol. Evol. 28: 2731–2739.

8. Saitou, N., and M. Nei. 1987. The neighbor-joining method: a new method for reconstructing phylogenetic trees. Mol. Biol. Evol. 4: 406–425.

9. Bennet, M., A. McCarthy, F. Dmitri, M. R. Edwards,..., F. Repp. 2014. A microscopy platform for correlative studies of tactic behaviors of microorganisms. PLoS One. doi: 10.1371/journal.pone.0101150.

10. Smith, M. J., P. E. Sheehan, ., L. J. Whitman. 2006. Quantifying the magnetic advantage in magnetotaxis. Biophys. J. 91:1098–1107.

11. Mazzag, B. C., I. B. Zhulin, and A. Mogilner. 2003. Model of bacterial band formation in aerotaxis. Biophys. J. 85:3558–3574.

Table S1: Parameter values used in the numerical calculations.

Parameter	**Value**	**Source**
Swimming speed v	20 μm × s^{-1}	This study
Switching rate (k_{RL} and k_{LR}), basal value	1/6 s^{-1}	(9)
Switching rate (k_{RL} and k_{LR}), increased value	1 s^{-1}	(9)
Oxygen consumption rate κ	0.01 fmol/min/cell	(10)
Oxygen concentration at which consumption is half maximal (c_a)	0.75 μM	(10)
Oxygen concentration at the open end	200 μM	This study
Preferred oxygen concentration (c_{opt})	2.5-3.5 μM	This study and (10)
Oxygen diffusion coefficient (D)	2100 $\mu m^2 \times s^{-1}$	(11)
Total number of bacteria	10^6	See text

TABLE S2 Speed motility (in µm/s) of the cells swimming in the anoxic or oxic zone surrounding the microaerotactic band. Cells swimming from the band toward the anoxic zone (purple), from the anoxic zone toward the band (light blue), from the band toward the oxic zone (red), and from the oxic zone toward the band (dark blue). Table shows the average velocities of eleven MTB depending on their swimming direction and their position compared to the microaerotactic band. Arrows indicate the significant increase (green), decrease (red) or stagnation (yellow) of the speed motility between the – and + directions in the oxic and anoxic zones.

Strain	-	+	-	+
LM1	18,6 ± 0,9	12,1 ± 1	20,7 ± 1,5	29,2 ± 4,6
MC1	54 ± 8,1	54,5 ± 5,1	119 ± 13,6	88,8 ± 11,8
MSR1	13,3 ± 1,1	13,5 ± 0,6	23,3 ± 2,9	15,3 ± 1,9
MV1	7,8 ± 1,3	5,9 ± 1	8,5 ± 2,3	3,6 ± 1,3
PR1	21 ± 3	20,1 ± 3,1	50,5 ± 5,3	35 ± 3,5
PR2	8,4 ± 2,1	6,1 ± 1,2	23,7 ± 3,6	14 ± 1,5
PR3	90,8 ± 7,2	81,7 ± 4,7	109,9 ± 13,2	94,9 ± 6,6
RS1	20,5 ± 1,8	22,1 ± 1,8	n.a. --	n.a. --
SS1	30,6 ± 14,8	40,8 ± 8,7	111,6 ± 21	93,9 ± 19,7
SS5	35,7 ± 2,9	24,7 ± 0,9	32,1 ± 2,2	29,8 ± 1,5
UT4	15,9 ± 1,3	14,3 ± 1	25,9 ± 1,4	23,1 ± 0,9

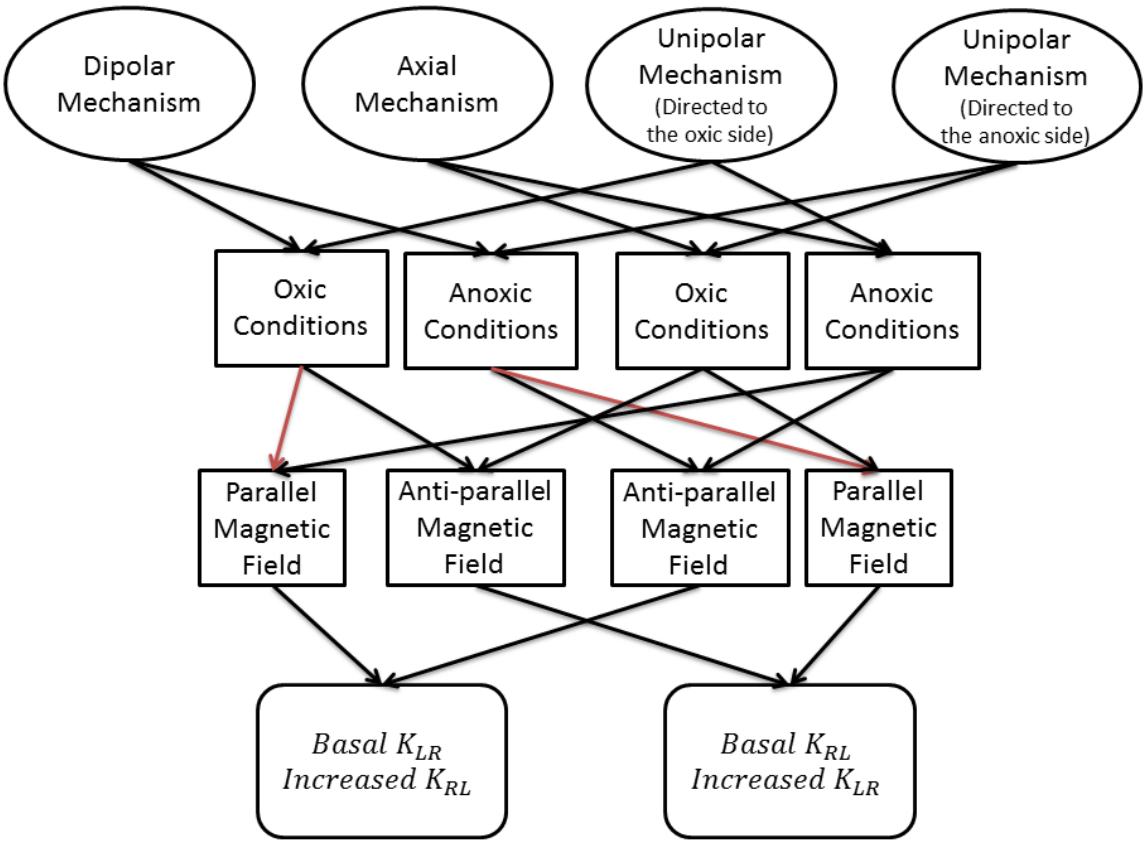

FIGURE S1 Diagram demonstrating how the switching rates for each mechanism were chosen. Red arrows represent paths that lead the cells to swim toward the wrong direction.

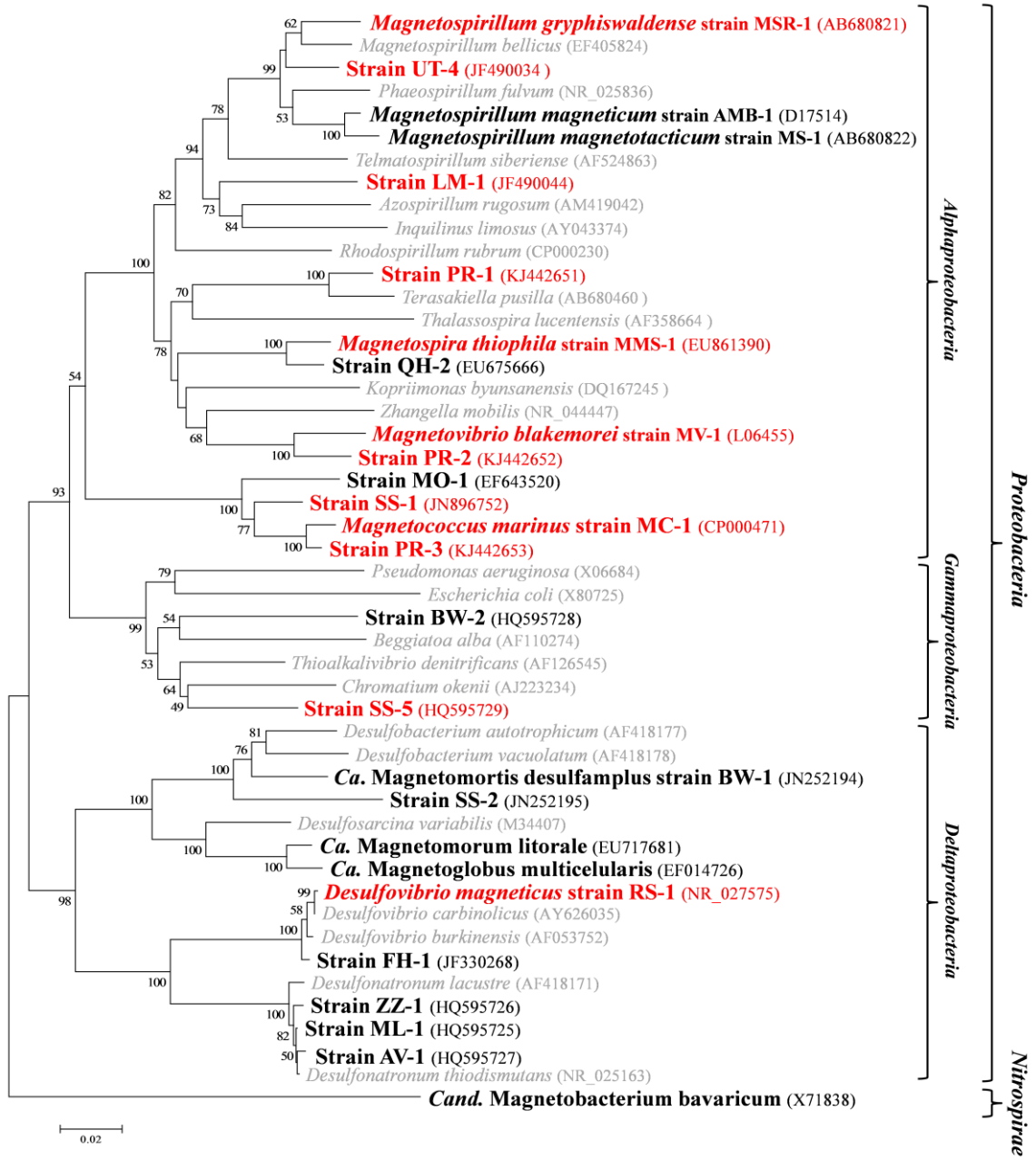

FIGURE S2 Phylogenetic positions of magnetotactic bacteria under study. Phylogenetic tree, based on 16S rRNA gene sequences using the neighbour-joining algorithm, showing the positions of the MTB under study (red), others MTB (black) and related non-magnetotactic bacteria (grey). Bootstrap values (higher than 50) at nodes are percentages of 100 replicates. Accession numbers are given in parentheses. Bar represents 5% sequence divergence.

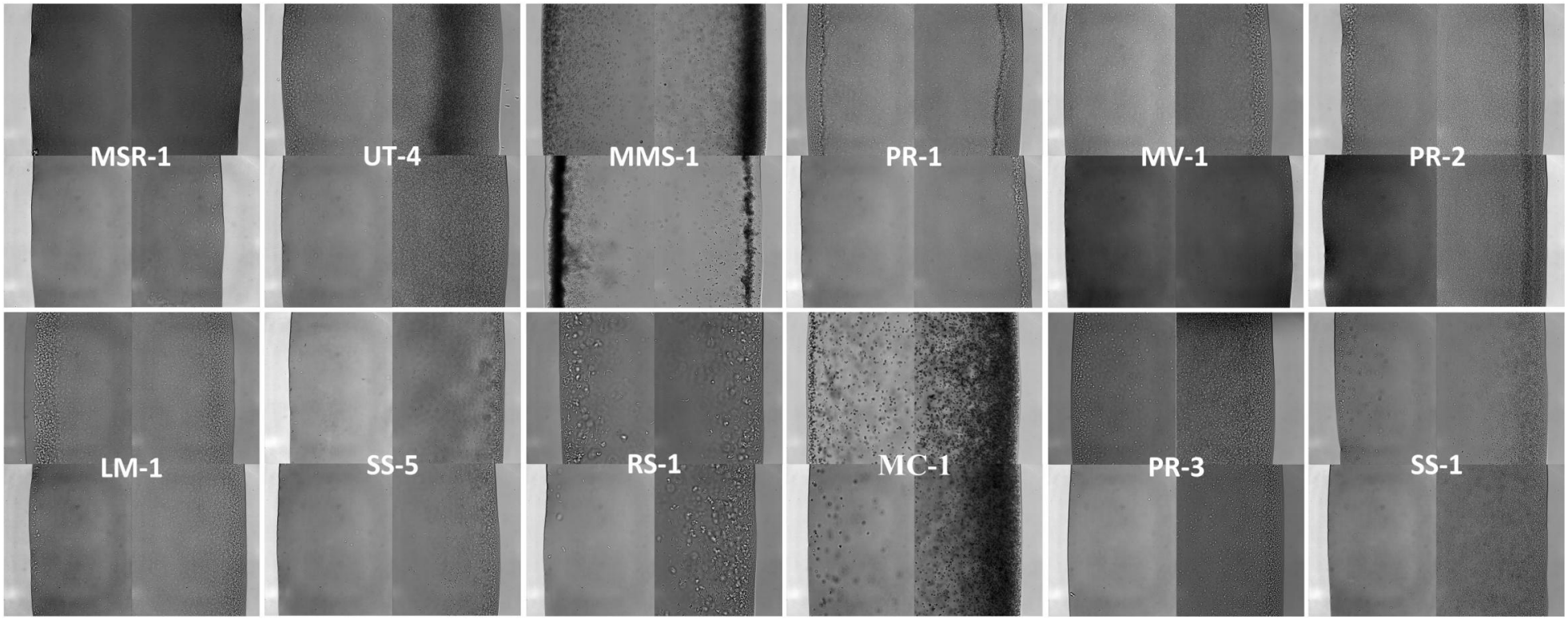

FIGURE S3 Observation of the magnetic behavior of twelve magnetotactic bacteria studied under the light microscope using the hanging drop technique. Before magnetic separation (top half of each panel), a majority of cells aggregate at the north side of the drop (upper right quadrant of each panel) whereas after magnetic separation (lower half of each panel) few or no south seeking cells remain, except for strain MMS-1 whose magnetic polarity is affected by the light of the microscope.

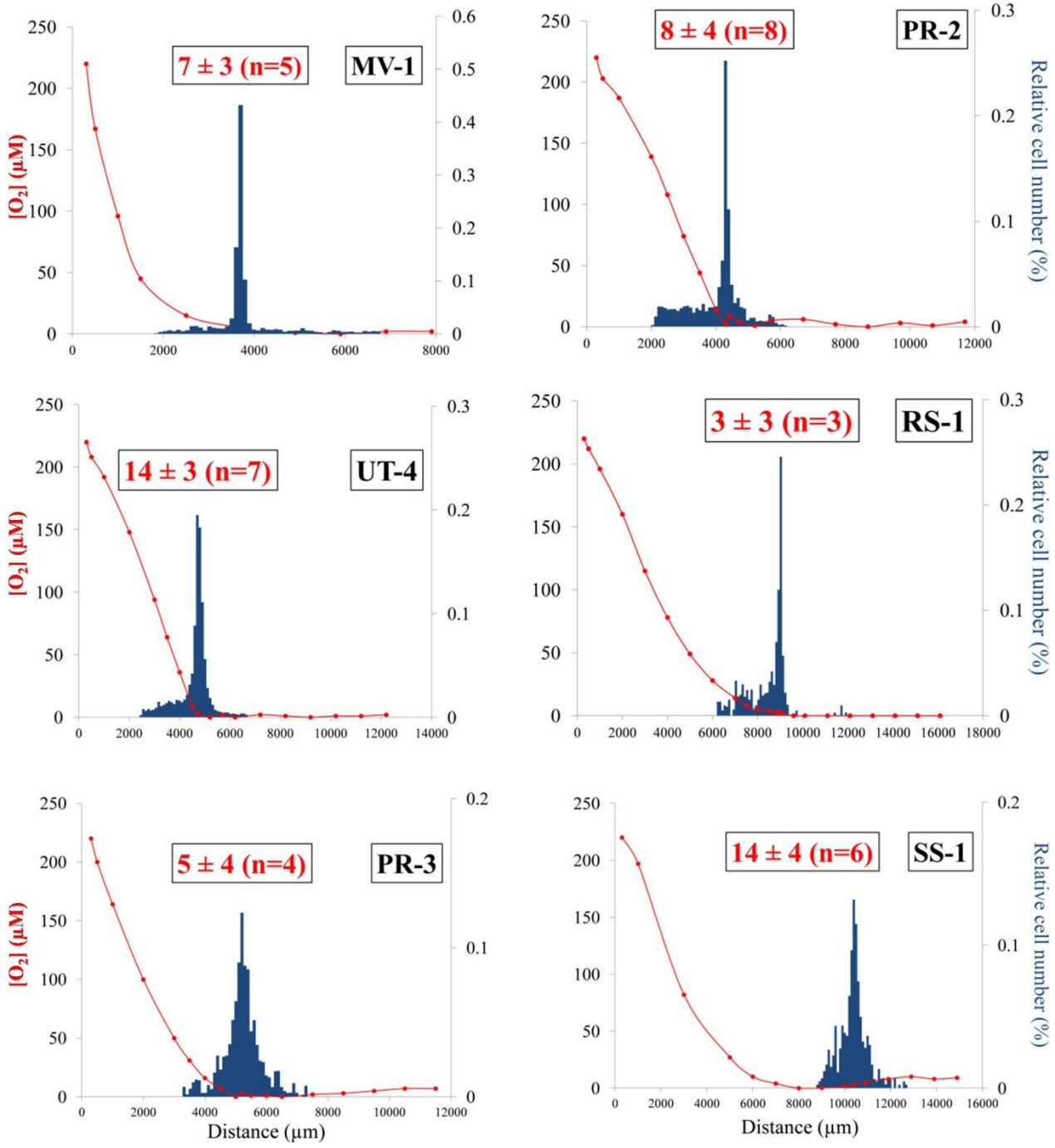

FIGURE S4 Relative cell distributions (blue histograms) of the twelve different magnetotactic bacteria under study in oxygen gradients (red circles). Each graph was made from a single microcapillary. Oxygen concentrations were obtained from one measurement at different positions along the capillary. In red is the value of the oxygen concentration (in µM) in the center of the aerotactic band (n represents the number of capillaries used to measure the average oxygen concentration at the band; see Materials and Methods for the error calculation). The relative number of cells were measured every 100 µm from triplicate counts. The same capillary was also used to measure the oxygen concentrations. For strain UT-4, the distribution of cells were determined from a total of 17,668 cells; for strain MV-1 from 2,252 cells; for strain PR-2 from 4,489 cells; for strain RS-1 from 265 cells; for strain PR-3 from 732 cells; and for strain SS-1 from 462 cells.

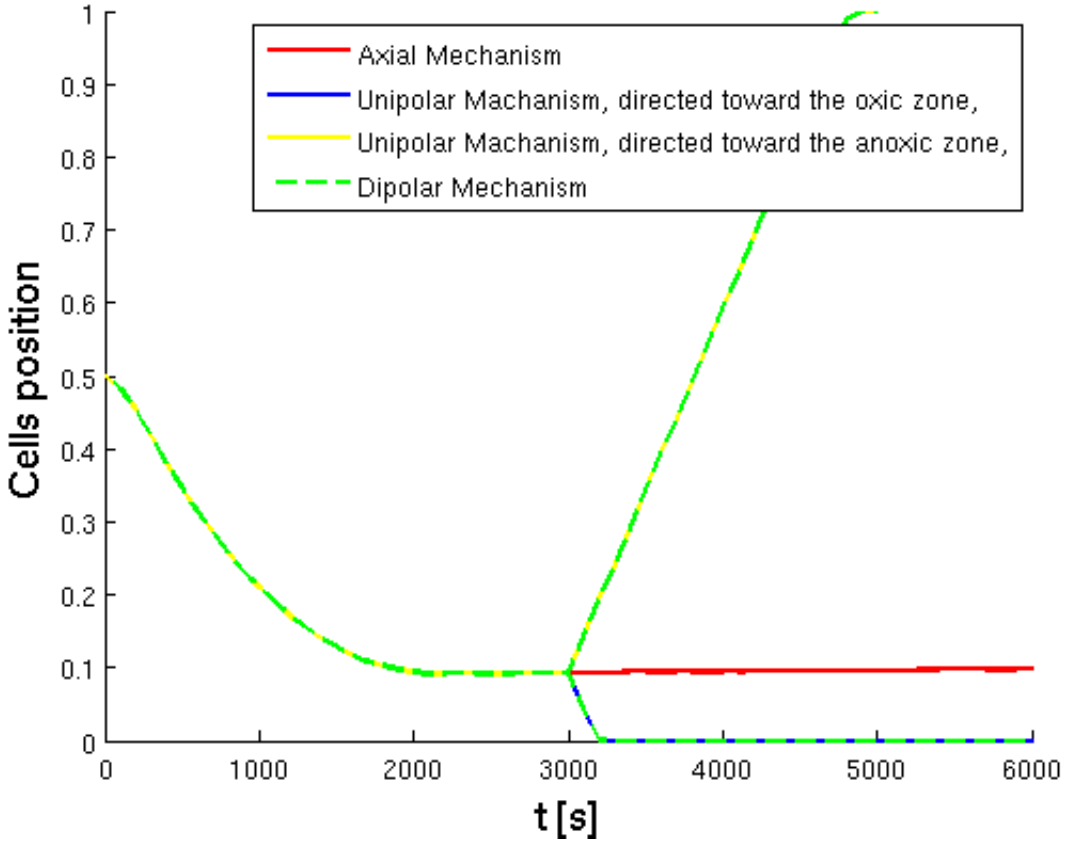

FIGURE S5 Relative position of the bacteria in the capillary while the band is formed and after the magnetic field is reversed (after 3000 s) for the different mechanisms. For the dipolar mechanism, after the reversal of the magnetic field, the positions of both bands are shown.

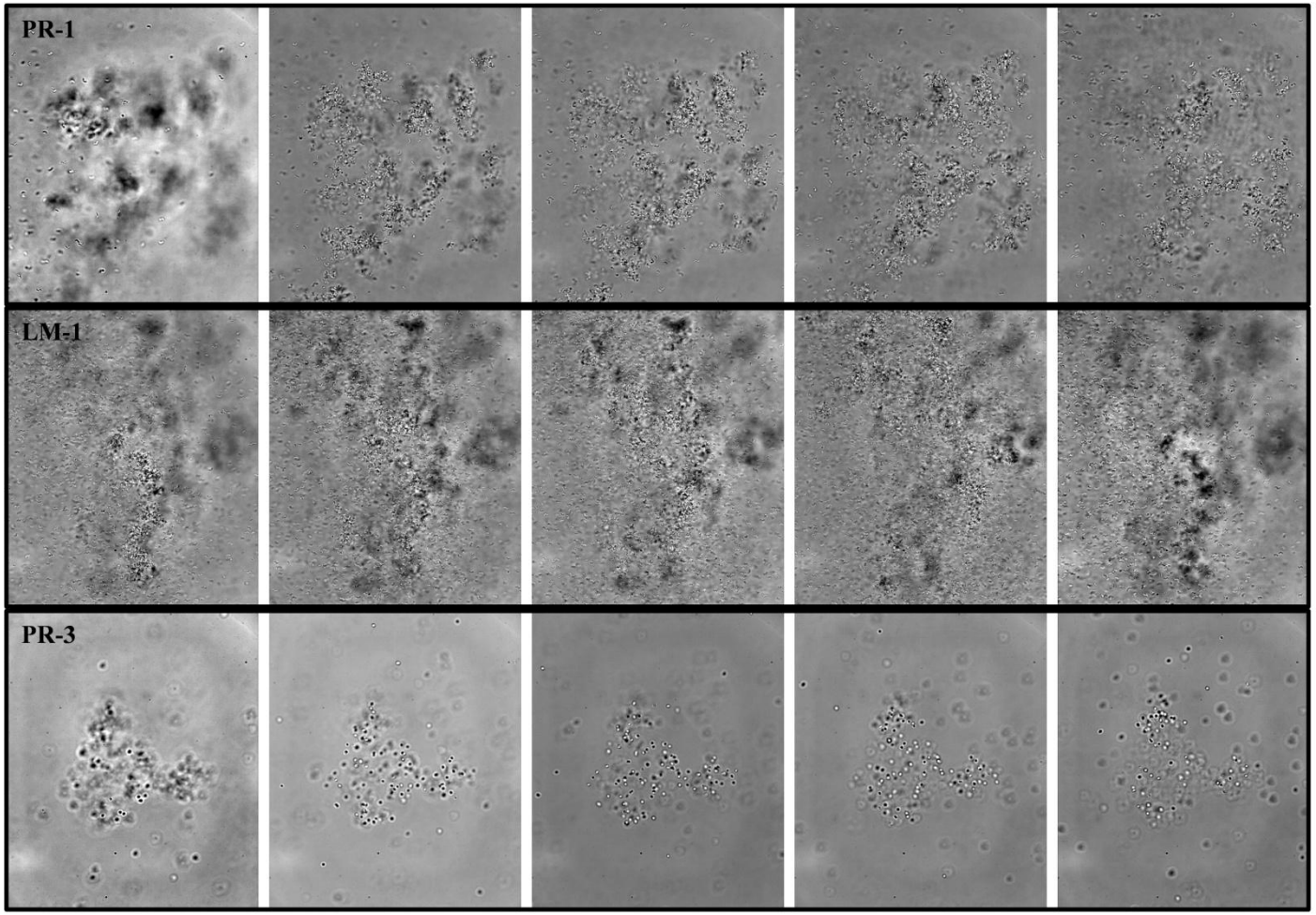

FIGURE S6 Formation of aggregates by strains PR-1, LM-1 and PR-3 at the oxic-anoxic interface, one hour after the formation of the microaerobic band. In each frames the different panels are separated by a distance of 5 µm in the Z axis.

MOVIE S1 Cells of strain SS-5 moving in the anoxic zone of the aerotactic band. Cells continue swimming back and forth along the magnetic field through the band. Once they reached the regions of too high or too low oxygen concentration, cells reversed their swimming direction without reorientation of the cell body.